JOURNAL OF PROPULSION AND POWER
Vol. 24, No. 4, July–August 2008

Computational Methodology for Carbon Monoxide Emission for Aeroengine Combustor Design

Michel Cazalens,* Matthieu Rullaud,† and Jean Philipe Frenillot‡
Société Nationale d'Etude et de Construction de Moteurs d'Aviation, 77750 Villaroche, France

DOI: 10.2514/1.33734

Design of lean combustion technologies will have to face the problem of the increasing difficulty to control carbon monoxide emission. To help the designer, a 91 species and 1329 elementary reactions chemical mechanism for Jet A1 kerosene is tabulated and coupled with the turbulent flow through a presumed probability density function approach. The capacities of the methodology for finite rate chemistry prediction are assessed by the computation of several operating conditions of an experimental combustor. The first case corresponds to high-power operating conditions and a good agreement is achieved between the predicted and measured carbon monoxide emissions and temperature profile at the combustor outlet. The second case corresponding to low-power operating conditions for which finite rate chemistry effects are important is focused on the study of carbon monoxide emissions variations with respect to the global fuel air ratio of the combustor, while keeping constant the inlet air mass flow rate and the airflow split. A detailed discussion is provided to carefully check the coherence of the obtained results, then the full relevance of this tabulated approach regarding the prediction of finite rate chemistry effects for turbulent combustion in aeronautical combustors with liquid injection is concluded.

Nomenclature

c	=	progress variable
$\tilde{k}$	=	kinetic energy of turbulence
P	=	probability density function
$\mathbf{u}$	=	velocity vector
Y_{CO2}	=	carbon dioxide mass fraction
Y_{CO}	=	carbon monoxide mass fraction
Y_i	=	mass fraction of species i
Y_i^{eq}	=	mass fraction of species i evaluated at chemical equilibrium conditions
Y_c	=	$Y_{CO} + Y_{CO2}$
Z	=	mixture fraction
$\tilde{\varepsilon}$	=	dissipation of turbulence kinetic energy
ρ	=	mass per unit volume
φ	=	$Y_c Y_c$
χ_i	=	scalar dissipation rate for species I
$\tilde{\Omega}_\varphi$	=	mean reaction rate for $\tilde{\varphi}$
$\tilde{\omega}_i$	=	Favres mean reaction rate for species i
$\tilde{\omega}_{Yc}$	=	Favres mean reaction rate for $\tilde{Y}_c$
$(\overline{F\|Z^*})$	=	conditional average to $Z = Z^*$ of the function F

I. Introduction

DEVELOPMENT of clean combustors has clearly become a main objective for all the aeroengine manufacturers because pollutant emissions need to be strongly reduced to minimize the impact of aviation on local air quality and climate change. The Advisory Council for Aeronautical Research in Europe has set Europe's ambitions. Compared with the state of the art for the year 2000, they consist in a reduction of 80% of Nox emissions and 50% of CO2 emissions to be achieved by 2020 without enhancing CO and soot emissions. Through several European and national research programs it has been clearly established that lean combustion can be considered a good strategy regarding the Nox emissions reduction goal. Basically, lean combustion is achieved by increasing the percentage of airflow rate affected to the injection system to 80% of the total mass airflow rate in the combustor. For standard combustors in service today, this ratio lies in the range of 20–22%. To satisfy operability constraints of the engine, such as combustion stability at low operating rate and altitude restart capabilities, lean combustion is usually implemented by means of staged combustion devices [1,2]. Two combustion zones are created: one is optimized regarding low operating rate performances (CO and unburned hydrocarbon emissions operability), and the other one is mainly optimized regarding high-power operating rate performances (Nox emissions and temperature profiles). To reduce combustor size and mass, the staged combustion functions have recently been integrated directly through the injection system, giving rise to a new generation of injection systems [1]. The staged combustion zones no longer result from the geometry of the combustor but from the topology of the aerodynamic flow generated by the different swirlers associated with the injection system and from the fuel spatial distribution. The technological problem lies in the optimization of fuel/air mixing at high-power operating rate to minimize the Nox emissions and, simultaneously, in the control of the air/fuel mixing at low-power operating rates to maintain CO and unburned hydrocarbons emissions at very low-level values. Unfortunately, basic design rules established from experience gained during the development of standard combustors (not staged) cannot be applied to the optimization of low-emissions combustors based on staged injection systems. Although the physical behavior of CO formation and oxidation is not changed by the technological strategy, there is not sufficient knowledge regarding staged combustors to turn into efficient and reliable design rules to control CO emissions during the design process. Global methods [3] can only be applied when the combustor has been well characterized and are useless for designing innovative low Nox combustors. When the engine is operated at high-power conditions, CO emissions can be computed reliably from equilibrium chemistry. Unfortunately, when the engine is operated at low-power conditions, CO emissions can be much greater than those measured at high power and cannot be evaluated from equilibrium calculations. Fuel placement regarding the mixing topology and structure is the main degree of freedom to control CO emissions [2,4]. Computational fluid dynamics (CFD) tools could appear to be the best solution to efficiently design such staged combustors, only if finite rate chemistry effects can be accounted for in a way that all the

Received 27 July 2007; revision received 16 March 2008; accepted for publication 16 March 2008.

*Combustion Design Reviewer, 2 Rond Point René Ravaud, Moissy Cramayel.
†Research Engineer, 2 Rond Point René Ravaud, Moissy Cramayel.
‡Ph.D. Student, 2 Rond Point René Ravaud, Moissy Cramayel.

design and optimization iterations remain feasible within a reasonable time delay. Although transported probability density function (PDF) methods have been widely applied to the simulation of reactive turbulent flows, with detailed chemistry [5–13] for laboratory flames to simple swirling ones, they will not be considered within this study, mainly because of their CPU time requirement and the lack of any fully reliable micromixing model over the large operating domain of aeronautical combustors. For example, inlet pressure can vary from 0.3 to 40 bar, inlet temperature can vary from 220 to 800 K, and the global equivalence ratio can vary from 0.5 to 4%. Therefore, large differences between combustion regimes could be encountered within this operating domain with very different coupling phenomena between detailed chemistry, transport phenomena, and turbulence [14]. Nox emissions and temperature profiles have been addressed in [15] for an aeronautical combustor but, unfortunately, nothing is said about the model's capacity to compute finite rate chemistry effects at low-power conditions. The present paper is dedicated to the capabilities demonstration of a Reynolds-averaged Navier–Stokes (RANS) CFD method based on presumed PDF, mainly applied to the computation of CO emissions. Section II highlights the studied configuration and the associated objectives. The numerical tools and models are presented in Sec. III , and a detailed discussion of the results is provided in Sec. IV. Some indications about future work are provided in Sec. V, and a general conclusion is proposed in Sec. VI.

II. Configuration and Objectives

The unique hardware configuration that has been considered is an experimental standard annular combustor (Fig. 1) burning kerosene (Jet A1) for which a complete characterization is available for several operating conditions. Gas analysis is used to measure the exit temperature profiles. This is performed by means of a rotating probe taking five samples at different radii, thus the entire outlet section is explored. Then, the various measured concentrations are processed to obtain the temperature profiles and averaged on the outlet section regarding the pollutants emission. As usual, only a sector corresponding to one injector will be computed. Depending on the operating parameters of the combustor, inlet pressure, inlet temperature, and global fuel/air ratio, the finite rate chemistry effects are more or less observable. As a first goal, the model will be assessed from the comparison of the computed temperature map and CO emissions at the combustor exit with the measured ones for situations where finite rate chemistry effects are minimized. The corresponding operating parameters are $P = 15$ bar, $T = 674$ K, and fuel air ratio $= 2.5\%$ (FAR $= 2.5\%$). The second goal of this study will consist in the assessment of the CFD combustion model for the prediction of CO emissions when the fuel flow is varied and for situations where finite rate chemistry effects have to be considered. The injection system is an aerodynamic one, operating with 2.3% pressure losses and delivering a good quality spray for all the fuel flow rates for which the measured Sauter mean diameter (SMD) is equal to 25 μ for all operating conditions. To focus purely on chemistry effects regarding CO emissions, a low-power and low-pressure operating rate of the combustor engine is then considered: $P = 3.2$ bar, $T = 425$ K. For this point, the inlet parameters such as pressure, temperature, and air mass flow rate have been kept constant, while the fuel mass flow rate is changed, leading to a global fuel air ratio increasing from 1 to 2%. As a consequence, the CO emissions variations with respect to the global equivalence ratio are representative, as much as possible, of the coupling of finite rate chemistry effects with the turbulent flow. Linked to aeronautical combustors design and analysis, the third objective will consist in giving a few examples of current problems and tradeoffs for which the use of the present CFD methodology is very valuable.

Fig. 1 Experimental annular combustor.

III. Models and Numerical Tools

Turbulence combustion interactions are taken into account by means of the presumed conditional moment (PCM) turbulent combustion model [16,17], for which extensive validations regarding very simple laboratory turbulent jet flames have already been obtained [16]. The PCM turbulent combustion model is based on prototypical laminar premixed tabulated flames for a given operating pressure and inlet temperature which are controlled only by the mixture fraction Z and by the reaction progress variable $c = Y_c/Y_c^{\mathrm{eq}}$ where $Y_c = Y_{\mathrm{CO2}} + Y_{\mathrm{CO}}$ [18]. Species mass fraction and reaction rates are then stored as functions of the two variables Z and c to constitute the flame prolongated intrinsic low-dimensional manifold (FPI-ILDM) lookup table which can be computed using very detailed chemical kinetics. Assuming statistical independence between Z and c, the mean species mass fractions are written as

$$\tilde{Y}_i = \int_0^1 \int_0^1 Y_i^{\mathrm{FPI}}(Z^*, c^*)\bar{P}(c^*)\tilde{P}(Z^*)\,\mathrm{d}c^*\,\mathrm{d}Z^*$$

A beta function is introduced to presume the two probability density functions from the first and second moment of their stochastic variables. The classical balance equations for $\tilde{Z}$ and $\tilde{Z}''^2$ are solved to presume $\tilde{P}(Z^*)$. The determination of $\bar{P}(c^*)$ from the following balance equations of $\tilde{Y}_c$ and $\tilde{\varphi}$ with $\varphi = Y_c Y_c$ requires more detailed consideration.

$$\bar{\rho}\frac{\partial \tilde{Y}_c}{\partial t} + \bar{\rho}\,\tilde{\mathbf{u}}\cdot\nabla\tilde{Y}_c = -\nabla.\bar{\tau}_{Yc} + \nabla.(\bar{\rho}D\nabla\tilde{Y}_c) + \bar{\rho}\tilde{\omega}_{Yc}$$

$$\bar{\rho}\frac{\partial \tilde{\varphi}}{\partial t} + \bar{\rho}\,\tilde{\mathbf{u}}\cdot\nabla\tilde{\varphi} = -\nabla.\bar{\tau}_{\varphi} + \nabla.(\bar{\rho}D\nabla\tilde{\varphi}) - 2\overline{\rho\chi}_{Yc} + 2\overline{\rho\Omega}_{\varphi}$$

with $\bar{\tau}_{\varphi} = (\overline{\rho\mathbf{u}\varphi} - \bar{\rho}\,\tilde{\mathbf{u}}\,\tilde{\varphi})$ and $\Omega_{\varphi} = Y_c.\omega_{Yc}$. The scalar dissipation term is modeled with the following equation [17]: $\overline{\rho\chi}_{Yc} = \bar{\rho}\cdot C_{\varphi}(\tilde{\varphi} - \tilde{Y}_C\tilde{Y}_C)/(\tilde{k}/\tilde{\varepsilon})$ with $C_{\varphi} = 0.5$. The mean reaction rates are computed as

$$\tilde{\omega}_{Yc} = \int_0^1 \int_0^1 \omega_{Yc}^{\mathrm{FPI}}(Z^*, c^*)\bar{P}(c^*).\tilde{P}(Z^*)\,\mathrm{d}c^*\,\mathrm{d}Z^*$$

$$\tilde{\Omega}_{\varphi} = \int_0^1 \int_0^1 c^* Y_c^{\mathrm{eq}}(Z^*)\dot{w}_{Yc}^{\mathrm{FPI}}(Z^*, c^*)\bar{P}(c^*).\tilde{P}(Z^*)\,\mathrm{d}c^*\,\mathrm{d}Z^*$$

Finally, starting from the evaluation of the conditional averages $(\overline{Y_c|Z^*})$ and $(\overline{Y_c'^2|Z^*})$, the links between Y_c first and second moments and the corresponding moments for the progress variable are established [17]. Compared with the infinitely fast chemistry approach, only two balance equations are added to the system. It is possible to reduce the number of equations to be solved a little more by neglecting the fluctuations of Y_c for a given value of the mixture fraction, then obtaining a first-order formulation. Thus, the conditional average $(\overline{Y_c|Z^*})$ is used to enter directly the FPI lookup table in such a way that

$$\tilde{Y}_i = \int_0^1 Y_i^{\mathrm{FPI}}(Z^*, (\overline{Y_c|Z^*}))\tilde{P}(Z^*)\,\mathrm{d}Z^*$$

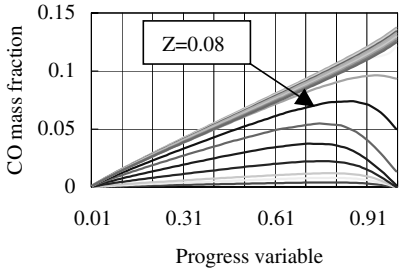

Fig. 2 Evolution of CO mass fraction for several mixture fractions.

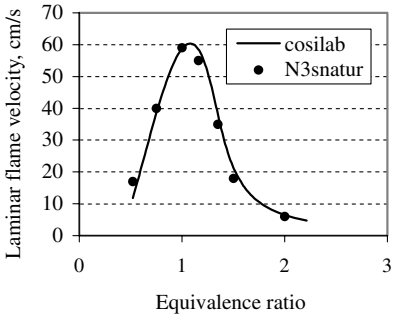

Fig. 3 Computed laminar flame velocities with detailed chemistry and molecular transport (Cosilab) and with the tabulated chemistry (N3snatur).

A complete description of the entire set of solved equations is given elsewhere [19] and will not be presented here. The liquid sheet atomization is not computed and fuel injection is represented by means of a crown synthetic injector representing the droplets statistics at the cup output. The size distribution is that of Rosin–Rammler and the evaporation rate is computed with a d square model, taking into account the droplet-heating phase. Forty thousand Lagrangian trajectories have been used for all the computations presented in this study.

IV. Results and Discussion

A. Tabulated Chemistry

Detailed chemistry for kerosene (Jet A1) is represented by 91 species reacting through a 1328 elementary reactions scheme validated for a pressure range of 1–10 bars [20] and for inlet temperature ranging from 300 to 1800 K. The molar composition of the model fuel representing Jet A1 is 74% $C_{10}H_{22}$, 15% C_9H_{12}, and 11% C_9H_{18}. Chemistry is tabulated through a collection of premixed flames computed for pressure and fresh mixture temperature corresponding to the low-power operating case of the combustor. The control parameters of the tabulated chemistry are the mixture fraction and the progress variable defined in Sec. III.

For a given inlet pressure and temperature, Fig. 2 displays the CO mass fraction as a function of the progress variable for a set of mixture fractions going from a lean, premixed flamelet to rich ones, for which the CO mass fraction does not decrease even when the progress variable is approaching one. For mixture fractions corresponding to lean and stoichiometric combustion, CO first increases with the progress variable before decreasing when the progress variable is sufficiently high. Figure 2 shows that the range of the progress variable values for which the CO mass fraction decreases is narrow compared with the one for which the CO mass fraction increases. The same situation occurs when the mixture fraction is considered. Outside the range of $Z = 0$ to Z around 0.080 (slightly over the stoichiometric values corresponding to $Z = 0.063$), it is not possible for the CO mass fraction to decrease. As a result, the mixture fraction and the progress variable appear to be parameters for which the corresponding probability density functions have to be determined very precisely in the physical space for the turbulent combustion computation to be reliable regarding CO emissions.

B. Relevance Assessment for the Tabulated Chemistry Control Parameters

The chemical kinetics that have been used in this study were obtained through a reduction of the complete Jet A1 oxidation mechanism involving 1800 reversible reactions and 225 species [20]. A part of the validation procedure for the reduced chemical mechanism consists in the comparison, for a set of inlet pressures, temperatures, and FAR, of the laminar premixed flame velocity, computed by means of the complete chemical scheme with the corresponding one computed by means of the reduced chemical mechanism [20]. The same kind of comparison has been performed here for a one-dimensional adiabatic situation. Figure 3 displays, as a function of the equivalence ratio, the laminar premixed flame propagation velocity that has been computed with the reduced mechanism by a specific code, taking into account detailed thermochemical and transport properties for all the 225 species involved (Cosilab). The laminar premixed flame velocity is then calculated by solving the laminar balance equation for the mixture fraction and for the progress variable for which the reactive term is computed from the tabulated chemistry (N3snatur). The laminar diffusion coefficients for the mixture fraction and the progress variable have been taken equal to 0.4 for all the N3snatur computed velocities. It represents an average of the individual species diffusion coefficients. Figure 3 proves that the comparison between the two computations is excellent for all the equivalence ratios. The coupling between species diffusion and chemical reaction that occurs naturally within a real flame, and which is computed when the reduced chemical mechanism is solved, is now very well reproduced when the tabulated chemistry is coupled with the flow through the mixture fraction and the progress variable. This good agreement demonstrates that the mixture fraction and progress variable are very relevant control variables to be used for further coupling of the tabulated chemistry with turbulent flow.

C. Model Assessment at High-Power Operating Conditions and Low Finite Rate Chemistry Effects

Three computations, corresponding to the high-power operating conditions, have been performed with the same RANS code. They differ by the combustion model used. The first computation uses a combustion model based on the infinitely fast chemistry hypothesis where the burning rate is only controlled by mixing and the temperatures are limited by the equilibrium ones [19]. The second and third computations, respectively, use the previously described PCM model at first and second orders.

As can be anticipated from the thermodynamic operating parameters (pressure, temperature, FAR), the measured quantity of emitted CO is very low (IECO = 3 g/kg) and therefore very difficult to be confidently calculated. At first order, IECO = 8 g/kg is computed, whereas, at the second order, the output is IECO = 5 g/kg. Nevertheless, the computed values appear to be in relatively good agreement with the measured ones because only the order of magnitude is searched for in this range of thermodynamic conditions. As finite rate chemistry effects appear to be very low, the progress variable fluctuations for a given value of the mixture fraction are believed to have limited effects on the predicted CO. However, the computed IECO (emission index of CO) with PCM at second order is closer to the measured value than the computed one with PCM at first order, which suggests that the progress variable fluctuations have to be taken into account even when finite rate chemistry effects are low. The influence of the PCM order on the computed IECO for situations in which finite rate chemistry effects are great will be studied in a detailed manner in Sec. IV.D.

Figure 4 displays the radial temperature distribution factor (RTDF) measured through gas analysis, with rotating probes plotted as a function of the aerodynamic vein radius at the high turbine nozzle inlet. Because of the finite dimension of the probes, it is not possible to measure temperatures near the wall at locations higher than 90% or lower than 10%. The computed temperatures at the walls strongly depend on the thermal boundary conditions representing the

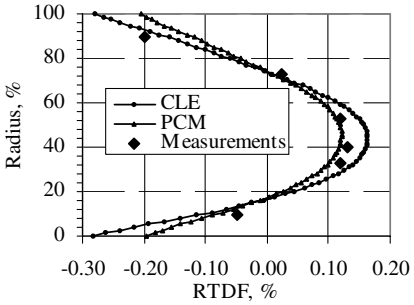

Fig. 4 Comparison of computed RTDF profiles with measured values.

effusion cooling efficiency and, because no measurements are available at those locations, we will only compare the computed and measured temperatures at the points corresponding to the probes radius. The six values of the RTDF profiles measured are plotted on Fig. 4 with symbols and will constitute the reference to assess the computational results. Obviously, the PCM computation provides a temperature profile in better agreement with the measured temperatures for all the points except for the one at 90%, which is substantially hotter, although it was correctly assessed with the combustion limited by equilibrium (CLE) model. Moreover, no difference can be observed for the temperature profile when the PCM computation order is changed. The PCM model, compared with the CLE results, reproduces very well the five other points. As mentioned previously, the CLE model provides temperatures limited by the equilibrium ones, therefore the difference of the computed temperatures from the measured ones for the three hottest points cannot be explained from possible dissociation effects because they are taken into account for the equilibrium temperature computations. This means that the infinitely fast chemistry hypothesis is not fully valid for these operating conditions and that finite rate chemistry effects have to be taken into account to compute reliable temperature profiles for the high-pressure turbine design. Nevertheless, as there is no visible difference on the temperature profile when the PCM order is changed, the impact of the progress variable fluctuation is found to be negligible, which is not the case when CO calculation is considered. Regarding the general shape and the radius of the maximum of the computed temperature profiles and the measured one, Fig. 4 indicates that they are very well reproduced by the CLE and PCM combustion models. Therefore, we can postulate that the common models for fuel injection, two-phase flow, turbulence, large-scale mixing through the mixture fraction balance equation, and small-scale mixing through the dissipation model for the mixture fraction fluctuations balance equation appear to be well adapted. No changes will be provided to that model for the following situations focused on high finite rate chemistry effects.

D. Model Assessment at Low-Power Operating Conditions and High Finite Rate Chemistry Effects

1. First-Order Probability Density Function Computations

For constant inlet pressure (3.2 bar), temperature (425 K), and air mass flow rate, the fuel air ratio is changed by varying only the fuel flow rate. Three experimental situations have been characterized in terms of CO emissions (Table 1), but to refine the prediction of IECO as a function of the fuel air ratio, five computations have been performed for which only the fuel mass flow has been changed, keeping constant all the others parameters. The comparison between measurements and computational results are reported in Table 1.

Table 1 Measured and computed IECO (first order)

FAR, %	IECO measured, g/kg	IECO computed, g/kg
1	71	35.6
1.25	——	47.1
1.5	45.2	49.8
1.75	——	44.8
2	38.2	38.5

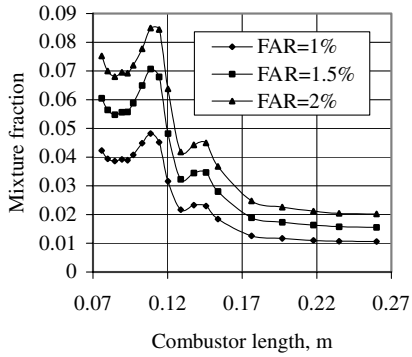

Fig. 5 Mixture fraction as a function of combustor length.

Obviously, the inlet pressure and temperature effects are well reproduced, because the computed IECO is much greater than the one obtained in the previous paragraph, and exhibits a correct order of magnitude. Nevertheless, the general experimental trend consisting in an IECO increase when fuel flow is decreased, keeping constant all the others parameters, does not appear when all the computed values are considered. For FAR > 1.5%, the trend is correct but, for lower fuel air ratio, a transition occurs and the variations of the computed values with respect to FAR are at the opposite of those observed experimentally. The first action that has been performed consisted of studying grid effect, thus the case for which FAR = 1% has been computed once again with a refined grid. The computed IECO is now equal to 34 g/kg and the trend remains the same. To investigate the computations in detail and to identify what could happen for the lowest equivalence ratios, the numerical results are presented as averages of relevant quantities computed along the combustor and over planes perpendicular to the axial direction from the output of the cup to the output of the combustor. To avoid overloading figures, only the results of the computations corresponding to 1, 1.5, and 2% for the FAR will be charted. Looking first at the mixture fraction, Fig. 5 indicates that the primary zone is globally entirely overstoichiometric for FAR = 2%, partially for the case of FAR = 1.5%, and globally understoichiometric for FAR = 1%. The impact of the additional air from the primary holes centered at 0.12 m and from dilution holes centered at 0.15 m is clearly visible. All of the mixture fraction values at the exit of the combustor are completely coherent with the targeted fuel/air ratio. A similar mixture fraction evolution is found for the three cases. This is coherent with the unchanged aerodynamic conditions at the inlet of the combustor and demonstrates that the FAR increase does not have a dramatic impact on large-scale mixing through the enhanced combustion and temperatures.

The energy reaction rate (Fig. 6) is representative of the global chemical scheme behavior that results from gaseous fuel/air mixing and from finite rate chemistry effects. Contrary to the mixture fraction rates, the energy reaction rate curves depend strongly on the

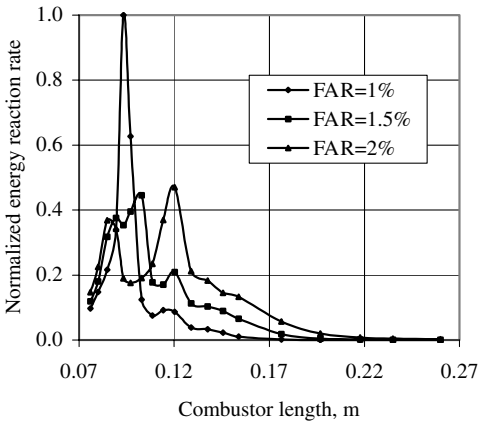

Fig. 6 Energy reaction rate as a function of combustor length.

FAR parameter. For FAR = 1%, fast mixing combined with sufficient available oxygen (remember that the primary zone has always understoichiometric conditions) lead to a narrow flame with high reactivity. When fuel is increased, the part of the aerodynamic energy required to mix fuel with air also increases. Because the total aerodynamic energy available remains unchanged, more time is needed to obtain flammable mixtures, and the chemical energy reaction rate is delayed in time and space as in the FAR = 1.5% case. Nevertheless, O2 is still present in sufficient quantities within the primary zone and the secondary peak centered at the primary holes location is still small. The situation is very different for the 2% case because the quantity of O2 is not sufficient for the combustion to be completed in the primary zone, and a secondary chemical energy reaction peak occurs when air from primary holes mixes with the hot mixture flowing out of the primary zone.

From Fig. 6, one can observe that no more chemical activity exists from $x = 0.22$ m to the output of the combustor, but the combustor length cannot be reduced. Usually, the remaining volume is dedicated either to the hot gases mixing to achieve an acceptable temperature profile at the high-pressure turbine inlet for the present case or to obtaining a sufficient combustion efficiency to overcome the inertia of the rotating parts of the engine when windmilling restart thermodynamics conditions are considered. In the primary zone, the temperatures along the combustor are strongly affected by the evaporation of injected fuel and by finite rate chemistry effects, nevertheless, they are as expected at the combustor output regarding the injected fuel/air. Because of residual droplet evaporation, shown by a slight increase of the mixture fraction at the vicinity of the dilution holes, all the temperature profiles show a secondary peak at this location (Fig. 7). The temperature increase along the combustor, associated with a constant inlet air mass flow rate, induces a corresponding mean axial velocity increase along the combustor (Fig. 8). At the combustor outlet, the maximum velocity is logically observed for the FAR = 2% case. The turbulent kinetic energy (Fig. 9) is maximum after the dilution holes and for the FAR = 1% case. Because the difference between the three cases begins to appear just after the primary zone, where most of the liquid fuel has been vaporized, temperature seems to be solely responsible through the increase of laminar viscosity, despite the fact that the mean velocity

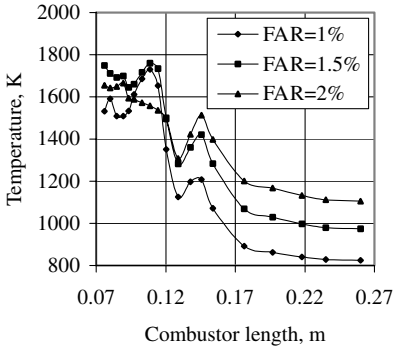

Fig. 7 Temperature as a function of combustor length.

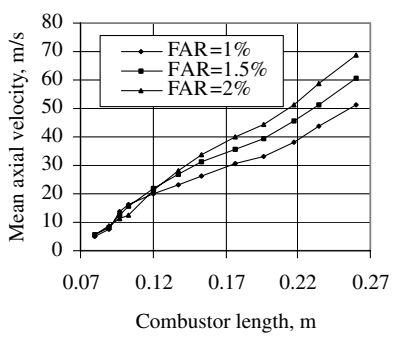

Fig. 8 Axial velocity as a function a combustor length.

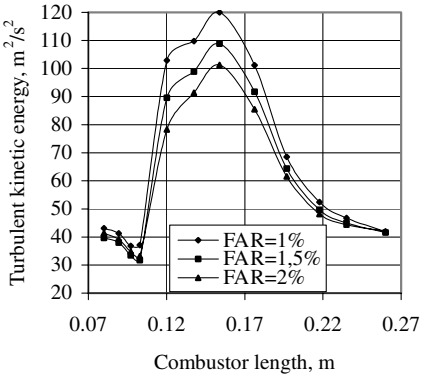

Fig. 9 Turbulent kinetic energy as a function of combustor length.

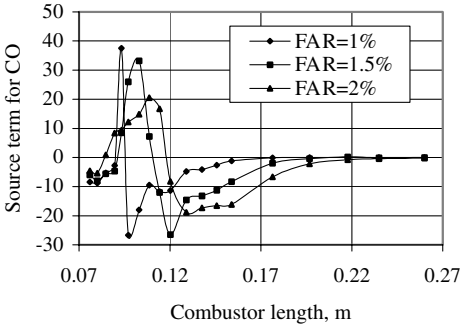

Fig. 10 CO reaction rate as a function of combustor length.

at the combustor output increases with the fuel/air ratio. The CO reaction rate displayed on Fig. 10 shows that production and consumption correspond to phenomena comparable in terms of intensity, but more and more separate in the physical space as the FAR is increased. Production of CO is restricted to the primary zone and the maximum of the production rate moves toward the output of the primary zone as FAR increases. The reaction rate for CO is equal to zero from $x = 0.22$ m to the combustor outlet and indicates that CO is in a steady state and suggests that the length of the combustor can be reduced without increasing CO emissions. The CO mass fraction (Fig. 11) confirms that large quantities of CO are produced within the primary zone, due to the lack of oxygen to complete the reaction for the highest FAR or due to temperatures that are too low for the leanest case. Globally, production and consumption have the same order of magnitude and lead to very small CO mass fractions at the combustor outlet where comparisons with measurement have to be performed. Figure 12 displays the progress variable evolution. The minimum only observed before the primary holes for the FAR = 2% case illustrates the lack of O2 to complete the chemical reaction, as already mentioned. For the other FAR values, after a dramatic increase before the primary holes, the progress variable is nearly

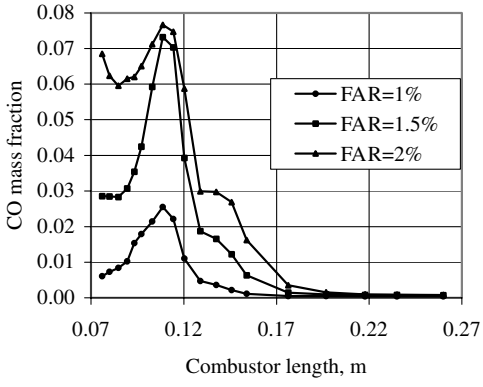

Fig. 11 CO mass fraction as a function of combustor length.

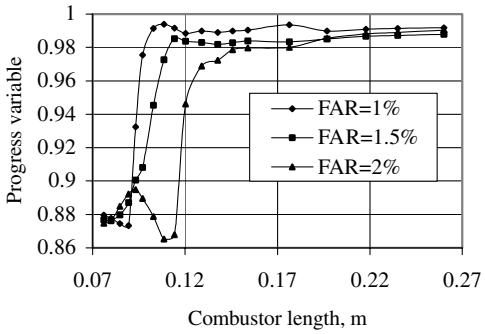

Fig. 12 Progress variable as a function of combustor length.

constant upon the combustor outlet. The progress variable value at the combustor output directly controls the CO mass fraction. From Fig. 12, it seems that this value depends on the slight progress variable evolution after the primary holes. Note that the measured trend for IECO regarding the cases of 1.5 and 2% can be obtained by our computations only because the FAR = 2% progress variable becomes larger than the FAR = 1.5% one after 0.20 m. For the FAR = 1% case, the progress variable remains greatest at the combustor outlet and therefore the computed IECO is minimum.

2. Second-Order Probability Density Function Computations. Influence of C_φ Constant

The balance equation for $\tilde{\varphi}$ is now solved. From tests on laboratory gaseous flames [17], $C_\varphi = 0.5$ was first retained, but unfortunately leads to the complete extinction of the combustor, then $C_\varphi = 1$ and $C_\varphi = 2$ were used and their impacts studied. Figure 13 displays the mixture fraction evolutions along the combustor axis and shows that there is no dramatic change between those computed with the first-order PCM models and those computed with the second-order model. Moreover, the influence of C_φ on mixture fraction evolution is predicted to be weak for the explored range of FAR, despite its high influence on the normalized energy reaction rate displayed by Figs. 14 and 15. As for the first-order computations, the targeted mixture fractions at the combustor output are achieved.

Figures 14 and 15 have been normalized with the same factor as Fig. 6 (first order) to allow direct comparisons between the different normalized reaction rates. For FAR = 1%, the most important effect lies in the decrease of the energy reaction rate intensity not fully compensated by an equivalent spatial enlargement of the energy curve that leads to a global decrease of the energy reaction rate. The greatest reduction is obtained for $C_\varphi = 1$ and corresponds to the situation where scalar dissipation is the lowest. The energy reaction rate is less affected for the FAR = 2% case, but a similar reduction in intensity is observed for $C_\varphi = 1$. As expected, changing C_φ induces substantial variations in the progress variable fluctuations (Fig. 16) and for CO (Fig. 17) for the two percentages. It appears from Fig. 16 that for a given C_φ the global FAR also strongly influences the progress variable fluctuations due to the reactive nature of the considered variable. Figure 18 displays the evolution of the progress

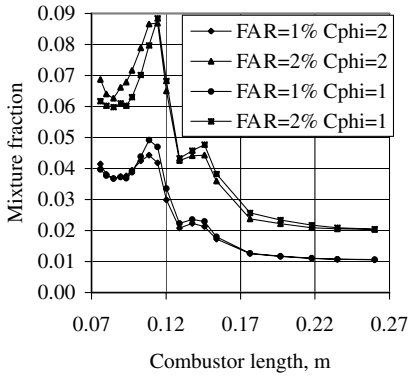

Fig. 13 Mixture fraction as a function of combustor length.

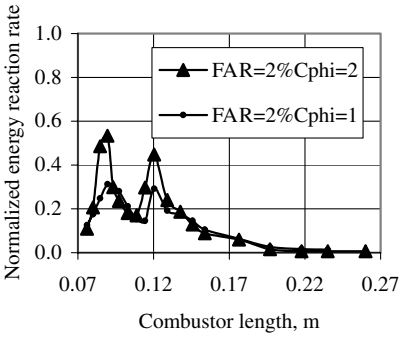

Fig. 14 Normalized energy reaction rate as a function of combustor length for FAR = 2%.

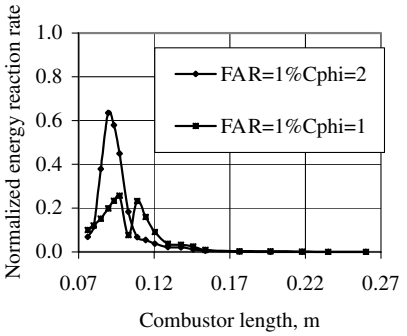

Fig. 15 Normalized energy reaction rate as a function of combustor length for FAR = 1%.

variables and shows that they are always lower and much more dispersed than the first order computation ones. This observation is coherent with the global diminution of the energy reaction rate. Combining Fig. 16 with Fig. 18 shows that the lowest values for the progress variable at the combustor output are associated with the highest fluctuation levels, and so increasing progress variable fluctuations acts as a delaying factor for the chemical reactions. This statement is confirmed by the fact that, as already mentioned, $C_\varphi = 0.5$ leads to the complete extinction of the combustor. Table 2 synthesizes the results of the various CO emissions computations. When $C_\varphi = 1$ is used, neither the trend nor the values are correctly reproduced, and large discrepancies are observed. When the fluctuations are reduced by the use of $C_\varphi = 2$, the cases corresponding to FAR = 1% and to FAR = 2% are correctly

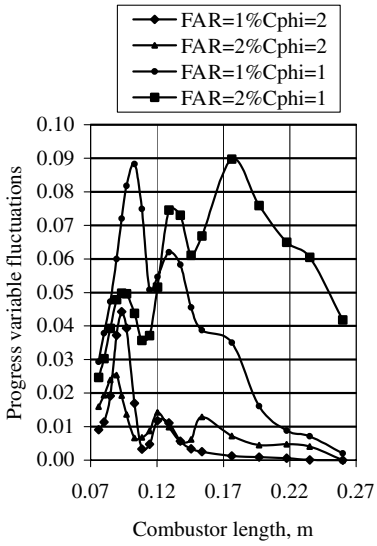

Fig. 16 Fluctuation of the progress variable as a function of combustor length.

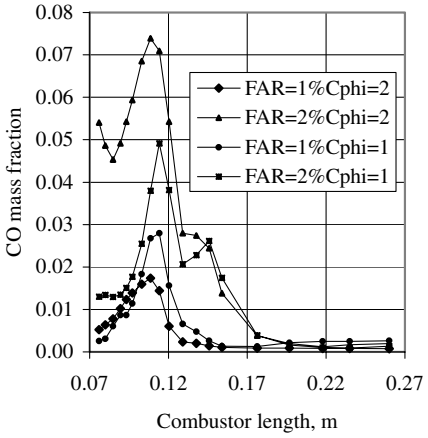

Fig. 17 CO mass fraction as a function of combustor length.

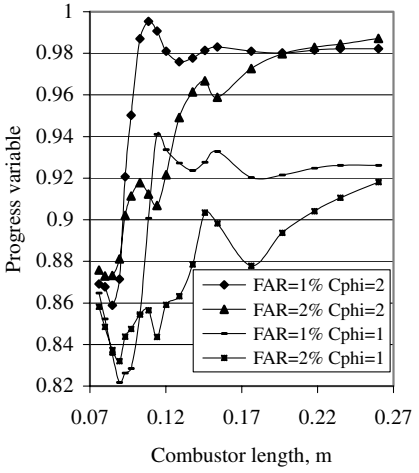

Fig. 18 Progress variable as a function of combustor length.

computed. Unfortunately, as for the first-order computation, the variation trend of IECO with FAR is no longer reproduced. It is to be noticed that, if the operating conditions corresponding to FAR = 1% or to FAR = 2% have been considered alone, the results obtained would have led to an erroneous positive conclusion regarding the capabilities of the global computation process and models.

Because the scalar dissipation rate is representative of the unresolved small-scale diffusion processes bringing species into contact at molecular level before combustion can occur, the computed CO emissions appear to be naturally totally dependent on the values assigned to C_φ. Our results suggest that a fixed value for C_φ is not adequate and that C_φ should vary at least within the computational domain and perhaps also regarding the global FAR, supposing that the global energy reaction rate can influence the small-scale mixing process. Vervisch et al. [17] indicate that C_φ should vary across the flame structure to reproduce direct numerical simulation results and that its exact determination is far from being straightforward. A dynamic model for the scalar dissipation rate of the progress variable fluctuations has been tested for a premixed turbulent flame stabilized by hot combustion products [21]. Nevertheless, as only comparisons regarding the main species CH4 and O2 are provided, no conclusions about minor species predictions can be set up for this model. Therefore, it seems that the second-order computations should only be considered for application on very simple laboratory flames for which the variation of combustion parameters are very limited. Because our goal consists of the computation of minor species emissions, such as CO, for aeronautical combustors with large variations of their operating parameters, first-order computations should be preferred. This situation could change if upstream research regarding scalar dissipation phenomena for reactive variable fluctuations in the presence of evaporating droplets leads to either a fully validated dynamic model for all the relevant parameters in the field of aeronautical combustion or a reliable rule for linking C_φ to some design parameters of the combustor (FAR, for example).

3. Influence of Droplets Sauter Mean Diameter with First-Order PCM Computations

The influence of the liquid phase has been investigated by varying the SMD of droplets from 15 μm to 50 μ. The measured SMD for the used injection system that corresponds to the same aerodynamic, nonreactive, operating conditions is equal to 25 μ. Obviously, changing the SMD leads to changes in the evaporation rate and of the droplets trajectories through interactions with the aerodynamic turbulent field. Therefore, the fuel mass source term placement within the combustor differs depending on the SMD. The results of the various first-order PCM computations are displayed in Fig. 19. They show that, due to a transition occurring for SMD > 30 μ, the experimental trend is now recovered, as well as the measured values for SMD = 35 μ. The SMD appears to be a relevant control parameter more valuable than C_φ, moreover, it can be reliably linked to the design parameters of the injection system. The interaction between evaporation, mixing, turbulence, and combustion with detailed chemical schemes is globally correctly reproduced. Nevertheless, the SMD used is different from the measured one in proportions superior to the measurement uncertainties. This leads to the conclusion that some improvement still has to be included in the two-phase flow description. If models for evaporation of multicomponent fuels and for a more precise description of the turbulent dispersion of droplets seem to be needed, the way that has been used to include the finite chemistry effect within turbulent reactive computations seems fully satisfactory. Figure 19 shows much more SMD effects on IECO for smaller FAR than for high FAR, and this effect should be directly linked with the global average temperature increase within the primary zone. When the global temperature increases within the primary zone, the CO emissions diminish because evaporation is faster, therefore mixing and combustion occur earlier and, because the mean chemical time is lower, the finite rate chemistry effects become less important. The high sensitivity of the computational results regarding small variations of SMD is coherent with the fact that small changes for the injection system lead to dramatic changes for pollutant emissions [2,4].

E. Calculations Exploitation Regarding a Few Examples Related to Aeronautical Combustor Design

Identification of relevant changes that can be brought to combustor design to control CO emissions cannot easily be achieved from measurements at the combustor outlet alone. Therefore, a great number of tests are needed to investigate the impact of some technological changes and to derive the appropriate correlations that will be used for design optimization. Notice that even the choice of the best correlation parameters is by itself a difficult problem. Using

Table 2 Measured and computed IECO (second order)

FAR, %	IECO measured, g/kg	IECO computed, g/kg, $C_\varphi = 1$	IECO computed, g/kg, $C_\varphi = 2$
1	71	266	70.7
1.5	45.2	250	106.2
2	38.2	113	40

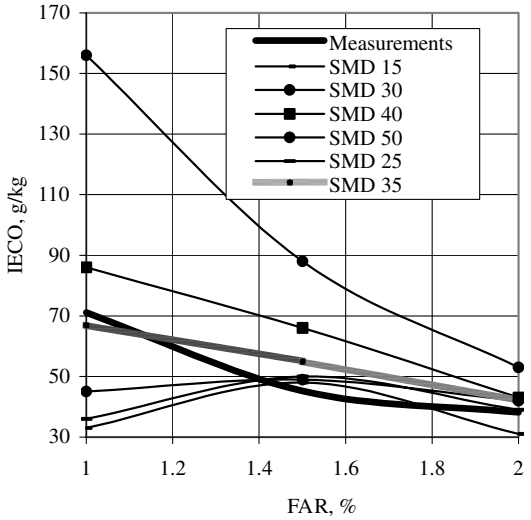

Fig. 19 CO emission index as a function of FAR for several SMD compared with measured ones.

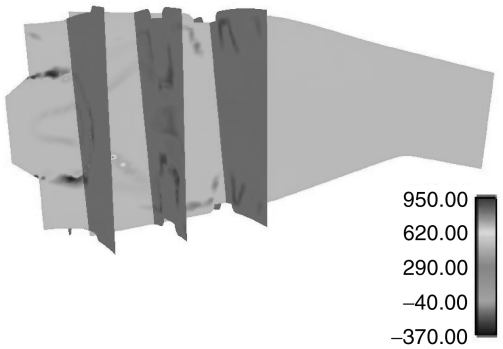

Fig. 20 CO reaction rate (arbitrary units).

validated CFD methodologies could change the situation by bringing very valuable information regarding first, the identification of relevant parameters from the understanding of the process and, second, the impact assessment of some variations for the chosen parameters with respect to CO emissions. A few examples of such possible changes that can be investigated by means of the presented CFD methodology are given hereafter. Figure 10 indicates that, for the most part, CO is formed very quickly within the primary zone of the combustor and gradually oxidized, in a second time, in the remaining part of the combustor or within the primary zone for the lowest FAR. Therefore, residence time and FAR within the primary zone appear as key parameters regarding CO formation. Keeping constant the global FAR and the residence time within the overall combustor, the FAR and the residence time in the primary zone can be affected by some variations brought to the airflow split to improve the altitude restart domain or to decrease the Nox emissions. The presented CFD methodology could therefore be used to solve the well-known tradeoff between Nox emissions/altitude restart domain/CO emissions. As already mentioned, Fig. 10 clearly shows that reducing the combustor length will have no impact on CO emissions because, from an abscise of 0.22 m to the outlet, the CO reaction rate is null. For the equivalence ratio representative of idle operating conditions (the two lowest ones considered within this study), the obtained results suggest that the CO formation rate could be varied by increasing the global mixing into the primary zone. Such an effect could be obtained by slightly increasing either the pressure losses through the liner or the swirl intensity. From the oxidizing part of the CO reaction rate, it is clear that moving the dilution holes upstream, as is done for the low-emission combustor to reduce Nox emissions, will impact the CO emissions. Figure 20 indicates that the cooling airflow for the wall has no effect on CO emissions for this combustor.

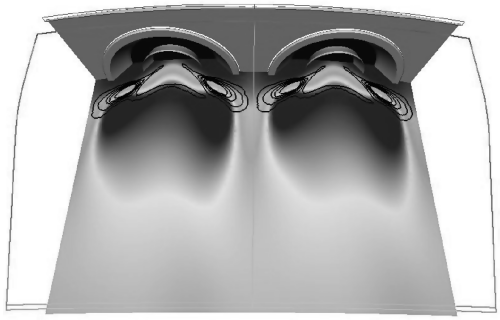

Fig. 21 Temperature map and iso-reaction rate for an ultra-low-Nox staged injection system.

CO production is not enhanced and CO oxidation is not stopped by the cooling airflow.

The PCM model is currently used to optimize staged injections. As an example, Fig. 21 displays the CO reaction rate that is part of a study dedicated to the assessment of the fuel split between the pilot and the full run circuit with respect to stability and emissions, while minimizing CO emissions.

V. Future Work

Although the first-order model described in the previous paragraph is considered fully validated and is currently used for the design of an ultra-low-Nox combustor, some complementary work and improvements seem still to be needed. As it has been shown that the two-phase flow parameters have a great influence on the first-order results, some investigations regarding the impact of changes to the droplet size distribution function, while keeping the mean Sauter diameter unchanged, will be undertaken. In a second step, the influence of the multicomponential nature of fuel for the evaporation rate will be considered. Moving to second-order formulation will become attractive only if it leads to more precise and more reliable calculations. Our results suggest that this situation could be obtained only by means of a combined work on the progress variable scalar dissipation rate modeling and on the progress variable fluctuations production and destruction by droplets. Derivations of reliable models are still needed for these phenomena. Obviously, large-scale mixing is of prime importance when fuel placement optimization is considered regarding the design of staged injection systems. To make progress with respect to this issue, the PCM model is currently integrated within a large-eddy simulation code that will allow one to carefully investigate the large-scale mixing impact on pollutants emissions for low-Nox combustion systems.

VI. Conclusions

Jet A1 kerosene tabulated detailed chemistry associated with a presumed PDF approach has been integrated within a RANS-CFD tool and successfully validated regarding the prediction of finite rate chemistry effects for aeronautical combustors design. For high operating conditions of the combustor, it has been found that taking into account finite rate chemistry effects leads to strong improvements of the temperature profile prediction at the combustor outlet compared with the classical infinitely fast chemistry approach. When low operating conditions of the combustor are considered, a good agreement between the measured and the computed CO emissions as a global FAR function is achieved when the SMD is slightly increased compared with the measured value. This methodology can now be used with confidence for the design of staged injection systems that will be part of ultra-low-Nox combustion systems.

References

[1] Cazalens, M., and Penanhoat, O., "Environmental Constraints and Appropriate R&T Strategy for Combustor Technology," *Proceeding of*

the 24th International Congress of the Aeronautical Sciences, International Congress of the Aeronautical Sciences Paper 300, 2004, ISBN 0-9533991-6-8.

[2] Cazalens, M., and Berat, C., "Fuel Atomisation, a Key Process for Aero Engine Combustors Design," *Proceeding of the 24th International Congress of Liquid Atomization and Spray Systems*, Inst. for Liquid Atomization and Spray Systems, Keynotes Lecture 2005-4, 2005.

[3] Allaire, D., Waitz, I. A., and Willcox, K. E., "Comparison of Two Methods for Predicting Emissions from Aircraft Gas Turbine Combustors," *Proceedings of the GT2007 ASME Turbo Expo: Power for Land, Sea and Air*, American Society of Mechanical Engineers, Paper 28346, 2007.

[4] Nakamura, S., McDonell, V., and Samuelsen, S., "Effect of Liquid-Fuel Preparation on Gas Turbine Emissions," *Proceedings of the GT2006 ASME Turbo Expo: Power for Land, Sea and Air*, American Society of Mechanical Engineers, Paper 90730, 2006.

[5] Magel, H. C., Schnell, U., and Hein, K. R. G., "Simulation of Detailed Chemistry in a Turbulent Combustor Flow," *Proceedings of the Combustion Institute*, Vol. 26, No. 1, 1996, pp. 67–74.

[6] Masri, A. R., Pope, S. B., and Dally, B. B., "Probability density function computations of a strongly swirling nonpremixed flame stabilized on a new burner," *Proceedings of the Combustion Institute*, Vol. 28, No. 1, 2000, pp. 123–131.

[7] Kraft, M., Stockelmann, E., and Bockhorn, H., "Analysis of Wet CO Oxidation Under Turbulent Non-Premixed Conditions Using a PDF Method and Detailed Chemical Kinetics," *Proceedings of the Combustion Institute*, Vol. 26, No. 1, 1996, pp. 807–813.

[8] Jones, W. P., and Prasetyo, Y., "Probability Density Function Modelling of Premixed Turbulent Opposed Jet Flame," *Proceedings of the Combustion Institute*, Vol. 26, No. 1, 1996, pp. 275–282.

[9] Kuan, T. S., and Lindstedt, R. P., "Transported Probability Density Function Modelling of a Bluff Body Stabilized Turbulent Flame," *Proceedings of the Combustion Institute*, Vol. 30, No. 1, 2005, pp. 767–774.
doi:10.1016/j.proci.2004.08.079

[10] Zhang, Y. Z., "PDF Method for Multidimensional Modeling of HCCI Engine Combustion: Effects of Turbulence/Chemistry Interactions on Ignition Timing and Emissions," *Proceedings of the Combustion Institute*, Vol. 30, No. 2, 2005, pp. 2763–2771.
doi:10.1016/j.proci.2004.08.236

[11] Lindstedt, R. P., Louloudi, S. A., and Vaos, E. M., "Joint Scalar Probability Function Modeling of Pollutant Formation in Piloted Turbulent Jet Diffusion Flames with Comprehensive Chemistry," *Proceedings of the Combustion Institute*, Vol. 28, No. 1, 2000, pp. 149–156.

[12] Saxena, V., and Pope, S. B., "PDF Calculation of Major and Minor Species in a Turbulent Piloted Jet Flame," *Proceedings of the Combustion Institute*, Vol. 27, No. 1, 1998, pp. 1081–1086.

[13] Harder, S., and Joos, F., "Modelling a Non-Premixed Industrial Gas Turbine Combustor by a Transported PDF Approach with ILDM Chemistry," *Proceedings of the GT2007 ASME Turbo Expo: Power for Land, Sea and Air*, American Society of Mechanical Engineers, Paper 27370, 2007.

[14] Hilbert, R., Tap, F., El-Rabii, H., and Thévenin, D., "Impact of Detailed Chemistry and Transport Models on Turbulent Combustion Simulations," *Progress in Energy and Combustion Science*, Vol. 30, No. 1, 2004, pp. 61–117.
doi:10.1016/j.pecs.2003.10.001

[15] Barths, H., Peters, N., Brehm, N., Mack, A., Pfitzner, M., and Smiljanovski, V., "Simulation of Pollutant Formation in a Gas-Turbine Combustor Using Unsteady Flamelets," *Proceedings of the Combustion Institute*, Vol. 27, No. 2, 1998, pp. 1841–1847.

[16] Rullaud, M., "Modélisation de la Combustion Turbulente via une Méthode de Tabulation de la Cinétique Chimique Détaillée Couplée à des Fonctions de Densité de Probabilité. Application aux Foyers Aéronautiques," Ph.D. Thesis, Inst. National des Sciences Appliquees, Rouen, France, 2004.

[17] Vervisch, L., Hauguel, R., Domingo, P., and Rullaud, M., "Three Facets of Turbulent Combustion Modelling: DNS of Premixed V-Flame, LES of Lifted Non Premixed Flame and RANS of Jet Flame," *Journal of Turbulence*, Vol. 5, No. 4, 2004, pp. 1–36.

[18] Fiorina, B., Gicquel, O., Vervisch, L., Carpentier, S., and Darabiha, N., "Approximating the Chemical Structure of Partially-Premixed and Diffusion Counter-Flow Flames Using FPI Flamelet Tabulation," *Combustion and Flame*, Vol. 140, No. 3, 2005, pp. 147–160.
doi:10.1016/j.combustflame.2004.11.002

[19] Ravet, F., Baudoin, Ch., and Schultz, J. L., "Modélisation Numérique des Ecoulements Réactifs dans les Foyers de Turboréacteurs," *Revue Générale de Thermique*, Vol. 36, No. 1, 1997, pp. 5–16.
doi:10.1016/S0035-3159(99)80061-0

[20] Luche, J., "Obtention de Modèles Cinétiques Réduits de Combustion. Application à un Mécanisme du Kérosène," Ph.D. Thesis, Laboratoire de Combustion et Systemes Reactifs, Orléans, France, 2003.

[21] Fiorina, B., Gicquel, O., Vervisch, L., Carpentier, S., and Darabiha, N., "Premixed Turbulent Combustion Modeling Using Tabulated Detailed Chemistry and PDF," *Proceedings of the Combustion Institute*, Vol. 30, No. 1, 2005, pp. 867–874.
doi:10.1016/j.proci.2004.08.062

J. Oefelein
Associate Editor